Carbon 119 (2017) 219–224

Contents lists available at ScienceDirect

Carbon

journal homepage: www.elsevier.com/locate/carbon

Hillock formation on nanocrystalline diamond

Felipe J. Valencia [a, c, e], Rafael I. González [b, c], Eduardo M. Bringa [d], Miguel Kiwi [a, c, *]

[a] Departamento de Física, Facultad de Ciencias, Universidad de Chile, Casilla 653, Santiago 7800024, Chile
[b] Faculty of Sciences, Universidad Mayor, Santiago, Chile
[c] Centro para el Desarrollo de la Nanociencia y la Nanotecnología, CEDENNA, Avda. Ecuador 3493, Santiago 9170124, Chile
[d] CONICET and Facultad de Ciencias Exactas y Naturales, Universidad Nacional de Cuyo, Mendoza 5500, Argentina
[e] Núcleo de Matemáticas, Física y Estadística, Facultad de Ciencias, Universidad Mayor, Manuel Montt 367, Providencia, Santiago, Chile

ARTICLE INFO

Article history:
Received 16 December 2016
Received in revised form
16 March 2017
Accepted 12 April 2017
Available online 15 April 2017

ABSTRACT

Hillock formation on nanocrystalline (nc) diamond under swift heavy ion irradiation is studied by means of classical molecular dynamics. The irradiation is simulated by means of a thermal spike model, the nc samples include as many as 5 millions atoms. Our results show that hillocks on nc diamond can be created for stopping powers (SP_e) in the range of 12–17 keV/nm, and grain sizes less than 13 nm. For smaller values of the SP_e only point defects are observed on the nc surface, while for larger SP_e hillocks suffer a transition to crater-rim, because of the increased sputtering that is due to the large energy that the ions deposit. We observe that the sputtering yields depend quadratically on the stopping power, contrary to what has been obtained by simulations for some single crystal solids. In addition, our results show that hillocks are smaller for 5 and 7 nm grain sizes, due to the large free volume that is available on the grain boundaries. Instead, for 10 and 13 nm the hillock is limited only to the amorphization of the grain closest to the surface. No hillock formation is expected for larger grain sizes, because of the transition of the nc to pristine diamond, where no hillock formation has been observed.

1. Introduction

The interaction of Swift Heavy Ions (SHI) with matter can generate structural transformations not only on the surface, but also in the bulk of the material [1]. The SHI interaction with carbon based materials is particularly relevant, because of the diverse uses it has found in optical [2] and electric devices [3], and in the sensor and energy industries [4,5].

As the SHI interact with matter energy is transferred and electronic excitations are created, which couple to the lattice and induce structural transformations along the SHI paths. Depending on the amount of energy transferred several scenarios are possible: from the formation of point defects [6], to the creation of fully amorphous regions [7,8], or to the emergence of craters [9], hillocks [10] to sputtering [11,12] of surface atoms, cluster melting and, for very large energies, partial or total cluster evaporation. The hillock formation mechanism is related to structural transitions due the large amounts of energy that the SHI deposit. These transitions reduce the track density, and consequently alleviate the induced stress, by means of the migration of matter towards the surface [13].

Among the carbon based materials SHI can create hillocks in diamond like carbon (dlc) [14–18], and in graphite [19,20], but they have never been seen in diamond. In fact, the diamond irradiation has been discussed in detail by various authors [14,21–23], and the largest stopping power (SP_e) measured corresponds to an irradiation with 1 GeV U ions (SP_e~49 keV/nm), which is not sufficient to create hillocks or amorphous paths in chemically vapor deposited diamond [14]. On the other hand, experiments by Chen et al. [4,5] in nano and micro-crystalline diamond have reported some structural transitions using a SP_e of 30 keV/nm, but only when the ion fluency is larger than a critical value.

Hillocks and craters in diamond, created by irradiation with highly charged ions, have been reported [24]. This way large and strongly localized electronic excitations are generated; on the other hand, using keV irradiation energies, where the nuclear SP predominates, mainly collision cascades are generated [25,26].

As of now a large amount of evidence shows that the use of nanocrystalline (nc) materials improves the radiation resistance, both in the nuclear [27] and in the electronic [28,29] regimes.

* Corresponding author. Departamento de Física, Facultad de Ciencias, Universidad de Chile, Casilla 653, Santiago 7800024, Chile.
E-mail address: m.kiwi.t@gmail.com (M. Kiwi).

http://dx.doi.org/10.1016/j.carbon.2017.04.020
0008-6223/

However, we previously studied, using molecular dynamics, a case where nc diamond displays large irradiation effects [30]. In fact, the track formation in nc diamond can be obtained with a SP_e of ~ 15 keV/nm in samples with grain sizes of ~ 5 nm. The explanation lies in the fact that the thermal conductivity of nano-diamond can diminish, by up to two orders of magnitude, compared to pristine diamond [31–33]. This way the latent track is precluded from efficiently dissipating the energy deposited by irradiation, and damage does result. Actually, this confinement due to the presence of grain boundaries, allows for a variation of the density along the nuclear track, due to the fact that the sp3 rich C bonds switch to sp2, in analogy to what was observed in dlc [15] and in nc diamond [3,4]. As a consequence of this local density change, and in the presence of a surface, the formation of hillocks in nano diamond, which up to date has not been observed in diamond like materials, could result.

In summary, we study the hillock formation on nc diamond under SHI irradiation, using molecular dynamics simulations in combination with the thermal spike model. Once the conditions for hillock formations are achieved, we investigate the effects due to the SP_e and grain size, in order to describe the hillock formation in nc diamond.

2. Method

Our simulations were carried out using the reactive bond-order AIREBO potential [34] as implemented in the LAMMPS code [35]. The nano-diamond targets were built by Voronoi tesselation [36]. The grain sizes are: 5 nm ($50a_0 \times 50a_0 \times 5a_0$), 7 nm ($70a_0 \times 70a_0 \times 21a_0$), 9 nm ($90a_0 \times 90a_0 \times 27a_0$), 10 nm ($100a_0 \times 100a_0 \times 30a_0$) and 13 nm ($130a_0 \times 130a_0 \times 42a_0$), where $a_0 = 3.57$ Å is the diamond lattice parameter. Smaller grain sizes have already been investigated to study the thermal properties of polycrystalline samples [37]. Since our samples are far from equilibrium they were relaxed, following the procedure of Valencia et al. [30], using periodic boundary conditions in order to allow for grain boundary accommodation. Initially a few atoms with high potential energy, related to near-overlap at the grain boundaries, are removed. Next the samples are relaxed by means of the conjugate gradient energy minimization method, in combination with an algorithm that modifies the box size (box relax) in LAMMPS [35]. This way the final configuration will have both a low potential energy, and will be a zero global pressure structure. After that the sample temperature is raised to 40% of the melting temperature (1800 K) under a zero pressure barostat during 10 ps, to facilitate grain boundary accommodation. Finally, the sample is cooled down to 300 K, and periodic boundary conditions along the *z*-axis are removed. The evolution of the nc continues during 50 ps, to allow for the free surface reconstruction.

The SHI track is modeled by means of a thermal spike model [30,37,38], that consists of a 2 nm cylinder orthogonal to the *xy* sample plane, which is given a high temperature. This thermal energy delivered to the atoms in the track of the incident ions has to be consistent with the effective desired SP_e. The resulting temperature is monitored by means of a velocity rescaling algorithm during the first 100 fs. Since the energy delivered to the atoms is rather large, events such as high energy collisions might lead to improper behavior of the time integrator. In order to address this

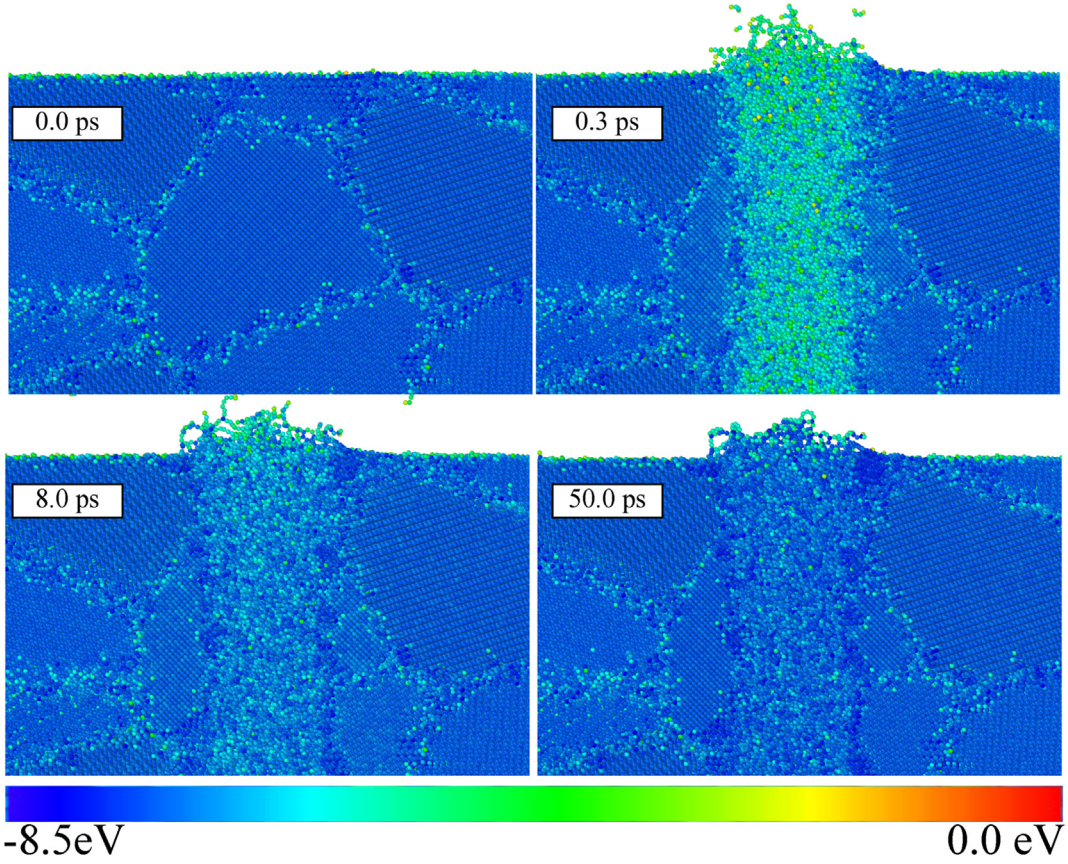

Fig. 1. Hillock on a 10 nm diamond sample at a $SP_e = 17$ keV/nm, after 20 ps irradiation. The color bar illustrates the potential energy of the C atoms. (A colour version of this figure can be viewed online.)

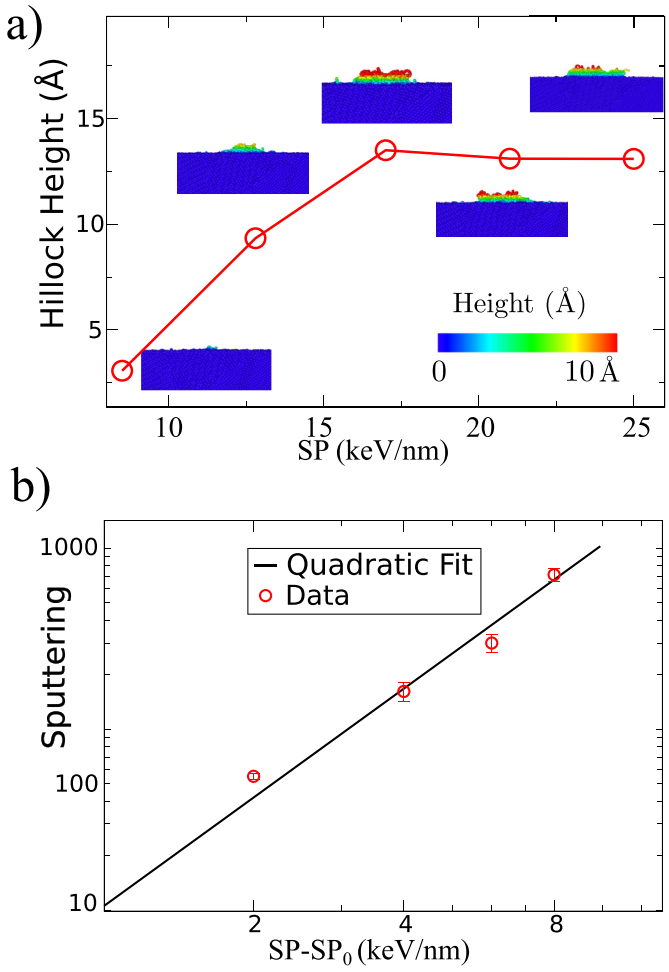

Fig. 2. a) Hillock height as function of SP_e for a 10 nm grain size sample. Color coding represents the height relative to the surface of the respective samples. b) Sputtering as function of SP_e; the blue line corresponds to a quadratic fit. SP_0 is 8.5 keV/nm. (A colour version of this figure can be viewed online.)

issue an adaptive time-step was adopted, which changes every time-step during the simulations, so that the atoms cannot move in excess of a fixed maximum distance. For these simulations we have established that a time-step between of 1.0 and 0.1 fs insures that the atoms do not move beyond 0.01 nm every time-step. After the heating of the track is over, the atoms are allowed to evolve using the energy conserving microcanonical ensemble, except for a thin boundary layer. These *xy* boundary atoms are connected to a Langevin thermostat, as implemented in LAMMPS [35], to keep the initial temperature constant at the boundaries, and to dissipate a possible shock wave due to irradiation; a damping parameter of 0.5 ps is used. The evolution of the thermal spike is followed during 50 ps to guarantee sample dissipation and cooling.

In general it is not possible to obtain experimental or theoretical values for the parameters of the thermal spike model. An efficiency of 0.2 for very different materials [39] and a track radius of 2 nm, similar to the ones used in dlc calculations, seem to be reasonable assumptions [39]. However, slightly different track sizes are expected to yield similar results. Simulations of both surface and bulk effects [40] use the same parameters. There are experimental indications of thin films bombardment which seem to be due to subtle surface effects, but such modeling is beyond the scope of this work [41]. In spite of the unsophisticated thermal spike we implemented it yields good agreement with dlc [15] and graphite experiments [6], as well as for silica [42], forterite [43] and MgO [44]. The targets were irradiated with an effective SP_e of 1.7, 2.6, 3.4, 4.2 and 5.0, which correspond to temperatures of 5000, 7500, 10000, 12500 and 15000 K, respectively. The relation between the effective and experimental SP_e is achieved by means of a 0.2 efficiency, which has proved to yield good agreement between simulation and experiment for dlc hillocks [15]. The SP_e covers a range from 8.5 to 25 keV/nm. To obtain representative results for each SP_e value four different nano-diamond samples were irradiated. Atoms that have *z* coordinates above the surface, and that are farther apart than the potential cutoff of any atom on the solid surface, are considered as sputtered away.

3. Results

The evolution of the thermal spike for a SP_e 17 keV/nm is shown in Fig. 1; it is observed that the energy transferred excites locally the atoms along the ion tracks giving rise to temperatures above the melting point of pristine diamond. As a consequence of the large deposited energy a radial shock wave propagates energy and momentum away, allowing for cooling of the track region. The large temperatures caused by irradiation increase the C atoms mobility, stimulating an sp3 to sp2 transition of their bonds. This transition takes place during the first picoseconds and is the one that allows for the formation of hillocks on the nano-diamond surface, due to the density decrease along the track, which is similar to what was observed in dlc [15]. This hillock is created at the very center of the thermal spike, and is confined within the grain that is irradiated directly. When the energy is large enough the hillock creation may be accompanied by surface sputtering. Due to the large diamond thermal conductivity the initial temperature profile disappears 10 ps after irradiation. Thereafter, that is up to 50 ps, the hillock remains unaltered.

Fig. 2a shows the hillock profiles as a function of SP_e for a target of 10 nm grains, indicating that for $SP_e < 10$ keV/nm only point defects are created, which emerge to the surface as isolated atoms. For SP_e~15 keV/nm small hillocks appear, but they do not reach above 1 nm in height. Both results are compatible with measurements [15] on dlc, where for SP_e~15 keV/nm features not higher than 1 nm were observed. While diamond has a much larger irradiation resistance than dlc there is an energy range where nc diamond can display a behavior similar to the one reported for dlc by Schwen et al. [15] The main difference is that for nc diamond and

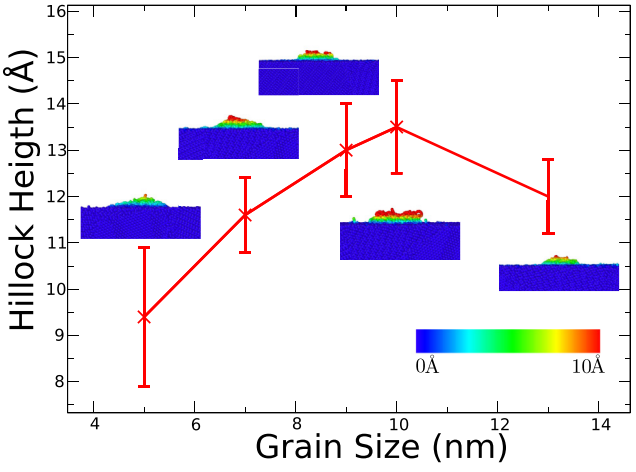

Fig. 3. Hillock height as a function of the grain size for $SP_e = 17$ keV/nm. The color bar represents the height relative to the surface. (A colour version of this figure can be viewed online.)

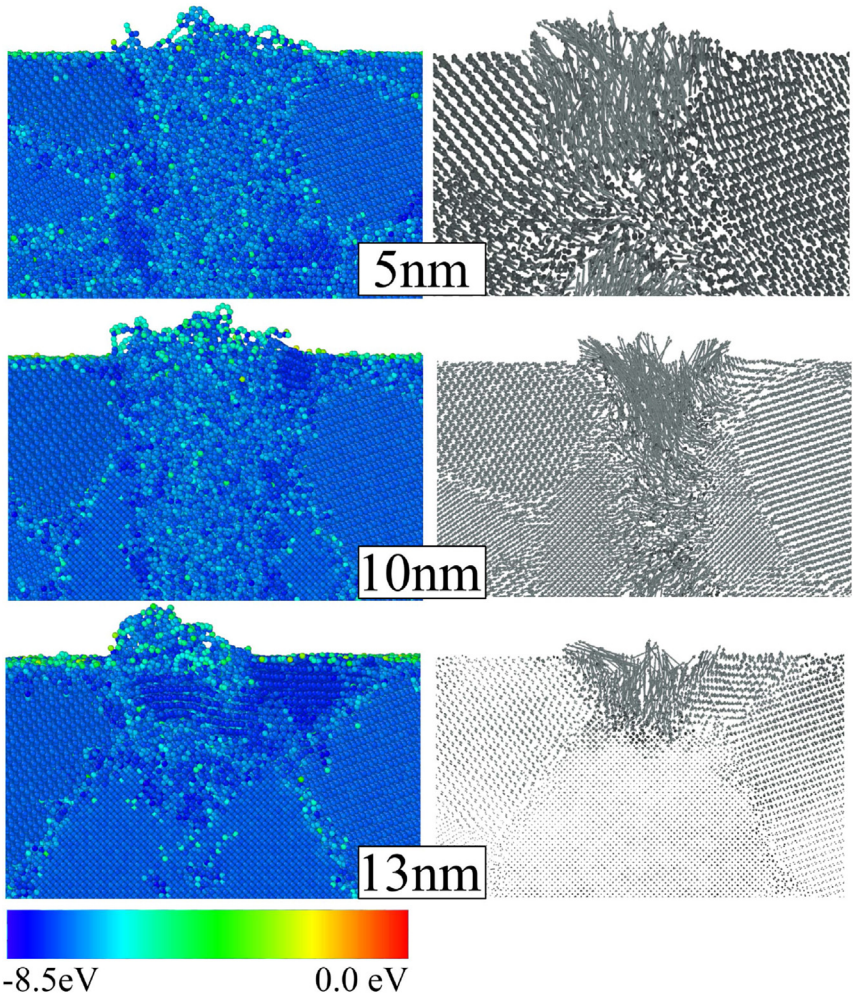

Fig. 4. Illustration of surface effects at $SP_e = 17$ keV/nm, for several grain sizes, of a 1 nm thick sample. The left panels show a lateral view of a cut across the sample; the color code illustrates the potential energy of the atoms in the sample. On the right hand side the vectors indicate the atomic displacements after 5 ps, relative to their initial positions, on the same sample cut. (A colour version of this figure can be viewed online.)

larger SP_e values the hillock height reaches a maximum beyond which a transition towards crater formation is observed.

Analytic thermal spike sputtering models predict a quadratic behavior as a function of stopping power [45]. However, MD simulations have shown that the inclusion of surface effects and pressure waves [46] reduces the stopping power dependence to linear in materials like a LJ solid or an EAM solid [47]. Fig. 2b displays a quadratic dependence of the sputtering yield as a function of stopping power, although analytic thermal spike sputtering models predict a quadratic behavior [45]. However, MD simulations have shown that the inclusion of surface effects and pressure waves [46] reduce the stopping power dependence to linear in LJ and EAM solids [47]. Covalent diamond bonding, and the confinement effect of the nanograins, might contribute to this stronger dependence. It is observed that the sputtering increases significantly for $SP_e \geq 15$ keV/nm. This increase quenches the formation of taller hillocks, mainly as a consequence of atom evaporation in the surface vicinity; actually, this mechanism generates the transition from hillock to crater-rim formation in nc diamond, for large SP_e.

Up to now we have limited our attention to the SHI surface damage of nc with grains 10 nm in size. Fig. 3 illustrates the role played by the grain size in the hillock formation in nano-diamond for a SP_e of 17 keV/nm. While in the bulk defect creation and amorphization is larger for smaller grain sizes, due to confinement effects, something completely different occurs on the surface. In fact, in Fig. 3 a larger hillock height is noticed as the grain size increases.

Inspection of the simulation results indicate that the formation of defects and amorphous regions is large for 5 and 7 nm grain size samples. However, these samples have a larger fraction of free volume, due to a significant presence of grain boundaries, which allow radial migration of material by reducing diffusion towards the surface. In Fig. 3 we observe a maximum hillock height for 10 nm nc grain size; beyond this size nc diamond tends to behave as pristine diamond, where hillock formation has not been observed [14].

The surface alteration due to irradiation, for different grain size samples, is shown in Fig. 4. The 5 nm radius nc sample leaves an amorphous track that widens slightly towards the interior of the nc; on the contrary, in the 10 nm radius nc the track is slightly wider on the surface, and in both cases the whole grain becomes completely amorphous due to irradiation. However, the 13 nm sample only exhibits point defects in its interior, a fact that is consistent with our previous report [30] on the irradiation of diamond nc. The confinement effect of small grains leads to slower energy dissipation from the hot track than for larger nc, promoting the formation of amorphous regions in 5 and 10 nm samples, as opposed to the formation of point defects in the 13 nm nc sample.

On the right panels of Fig. 4 the displacement vectors of the C atoms close to the surface, relative to their initial positions, are illustrated. For 5 and 10 nm the atoms diffuse at random inside the sample, with a preferential tendency to move towards the surface when the portion of the track is in its vicinity. But, for the 13 nm sample we observe that there is no significant atomic motion inside the fast cooling track, and point defects do not play any major role in hillock formation. The main contribution to hillock formation on the 13 nm sample is the amorphization of part of the grains closest to the surface.

The response to irradiation is not limited to increased atomic displacement; it also can generate the displacements of whole nc grains, as shown in Fig. 4, a tendency most marked in the 5 nm case where all the grains close to the track are displaced from their original positions. This fact may obstruct the diffusion of the atoms to the surface leading to the formation of lower height hillocks.

4. Summary and conclusions

The hillock formation in diamond had not been studied in detail due to its remarkable resistance to radiation. In fact, SP_e~50 keV irradiation does not cause amorphous tracks or hillock formation [14]. However, here we show that it seems possible to create hillocks in nano-diamond under $SP_e \leq 17$ keV/nm in samples smaller than 10 nm, a limit that is easily reached experimentally.

Hillocks are created during the first few irradiation picoseconds, by means of sp3 to sp2 conversion, similar to what Schwen et al. [15] observed in dlc. While dlc shows a linear relation between hillock height and energy loss ($SP_e \leq 70$ keV/nm), in nano-diamond the height reaches a limit due to the appearance of a hillock at the crater-rim. This diminished resistance to irradiation may be related to the strong reduction of thermal conductivity when grain boundaries are present [31,32]. However, in spite of the increase in radiation response nano-diamond with grains 5 and 7 nm in diameter showed an inverse effect, which leads to the formation of lower hillocks as compared to 9, 10 and 13 nm diameter samples. In addition, SHI irradiation induces a displacement of the surrounding grains, which may reduce the diffusion of material towards the surface. Larger grains display a transition from amorphous tracks to point defects, this way leading to a deformation limited to the grains closest to the outer surface. Simulations of larger grain sizes can provide additional information on the transition from nc to pristine diamond, where hillocks have not been observed. Surface effects on single crystal diamond have been looked for without success [6,14]. However, large hillocks have been found in amorphous diamond-like carbon [15]. Recent work on nanocrystalline diamond [4,5] did not look for surface effects. However, we expect that experiments performed with the techniques implemented by Schwen et al. [15] could succeed in the detection of the hillocks we found in our simulations.

Acknowledgments

EMB thanks useful comments by D. Schwen, P. Erhart, and K. Nordlund, and support from PICT-2014-0696 (ANPCyT), a SeCTyP-UN Cuyo under Grant M003. This work was supported by the Fondo Nacional de Investigaciones Científicas y Tecnológicas (FONDECYT, Chile) under grants #1160639 and 1130272 (MK), and Financiamiento Basal para Centros Científicos y Tecnológicos de Excelencia FB-0807 (RG, FV, JM, and MK). MK was supported by AFOSR Grant FA9550-16-1-0122. FV was supported by CONICYT Doctoral Fellowship grant #21140948.

References

[1] S. Talapatra, P. Ganesan, T. Kim, R. Vajtai, M. Huang, M. Shima, G. Ramanath, D. Srivastava, S. Deevi, P. Ajayan, Irradiation-induced magnetism in carbon nanostructures, Phys. Rev. Lett. 95 (9) (2005) 097201.
[2] A. Grill, Electrical and optical properties of diamond-like carbon, Thin solid films 355 (1999) 189–193.
[3] R.S. Sussmann, CVD Diamond for Electronic Devices and Sensors, vol. 26, John Wiley & Sons, 2009.
[4] H.-C. Chen, S.-S. Chen, W.-C. Wang, C.-Y. Lee, J. Guo, I.-N. Lin, C.-L. Chang, The potential application of ultra-nanocrystalline diamond films for heavy ion irradiation detection, AIP Adv. 3 (6) (2013) 062113.
[5] S.-S. Chen, H.-C. Chen, W.-C. Wang, C.-Y. Lee, I.-N. Lin, J. Guo, C.-L. Chang, Effects of high energy Au-ion irradiation on the microstructure of diamond films, J. Appl. Phys. 113 (11) (2013) 113704.
[6] D. Schwen, E. Bringa, Atomistic simulations of swift ion tracks in diamond and graphite, Nucl. Instrum. Methods Phys. B 256 (1) (2007) 187–192.
[7] J.-H. Zollondz, J. Krauser, A. Weidinger, C. Trautmann, D. Schwen, C. Ronning, H. Hofsass, B. Schultrich, Conductivity of ion tracks in diamond-like carbon films, Diam. Relat. Mater. 12 (3) (2003) 938–941.
[8] J.-H. Zollondz, D. Schwen, A.-K. Nix, C. Trautmann, J. Berthold, J. Krauser, H. Hofsass, Conductive nanoscopic ion-tracks in diamond-like-carbon, Mater. Sci. Eng. C 26 (5) (2006) 1171–1174.
[9] A. Tripathi, A. Kumar, F. Singh, D. Kabiraj, D. Avasthi, J. Pivin, Ion irradiation induced surface modification studies of polymers using SPM, Nucl. Instrum. Methods Phys. B 236 (1) (2005) 186–194.
[10] F. Aumayr, S. Facsko, A.S. El-Said, C. Trautmann, M. Schleberger, Single ion induced surface nanostructures: a comparison between slow highly charged and swift heavy ions, J. Phys. Cond. Mater. 23 (39) (2011) 393001.
[11] M. Toulemonde, W. Assmann, C. Trautmann, F. Gruner, H. Mieskes, H. Kucal, Z. Wang, Electronic sputtering of metals and insulators by swift heavy ions, Nucl. Instrum. Methods Phys. B 212 (2003) 346–357.
[12] F. Pawlak, C. Dufour, A. Laurent, E. Paumier, J. Perrière, J. Stoquert, M. Toulemonde, Carbon sputtering of polymer-like amorphous carbon by swift heavy ions, Nucl. Instrum. Methods Phys. B 151 (1) (1999) 140–145.
[13] A. El-Said, W. Meissl, M. Simon, J.C. López-Urrutia, C. Lemell, J. Burgdorfer, I.C. Gebeshuber, H. Winter, J. Ullrich, C. Trautmann, et al., Potential energy threshold for nano-hillock formation by impact of slow highly charged ions on a CaF 2(111) surface, Nucl. Instrum. Methods Phys. B 258 (1) (2007) 167–171.
[14] J. Krauser, J.-H. Zollondz, A. Weidinger, C. Trautmann, Conductivity of nanometer-sized ion tracks in diamond-like carbon films, J. Appl. Phys. 94 (3) (2003) 1959–1964.
[15] D. Schwen, E. Bringa, J. Krauser, A. Weidinger, C. Trautmann, H. Hofsass, Nano-hillock formation in diamond-like carbon induced by swift heavy projectiles in the electronic stopping regime: experiments and atomistic simulations, Appl. Phys. Lett. 101 (11) (2012) 113115.
[16] C. Rotaru, F. Pawlak, N. Khalfaoui, C. Dufour, J. Perrière, A. Laurent, J. Stoquert, H. Lebius, M. Toulemonde, Track formation in two amorphous insulators, vitreous silica and diamond like carbon: experimental observations and description by the inelastic thermal spike model, Nucl. Instrum. Methods Phys. B 272 (2012) 9–14.
[17] J. Krauser, H.-G. Gehrke, H. Hofsass, C. Trautmann, A. Weidinger, Conductive tracks of 30-MeV C 60 clusters in doped and undoped tetrahedral amorphous carbon, Nucl. Instrum. Methods Phys. B 307 (2013) 265–268.
[18] J. Krauser, A. Nix, H. Gehrke, C. Trautmann, A. Weidinger, et al., Highly conductive ion tracks in tetrahedral amorphous carbon by irradiation with 30? MeV C60 projectiles, New J. Phys. 13 (8) (2011) 083023.
[19] P. Nagy, B. Szabo, Z. Szabo, K. Havancsak, L. Biro, J. Gyulai, A model for the hillock formation on graphite surfaces by 246MeV Kr+ ions, Ultramicroscopy 86 (1) (2001) 31–38.
[20] K. Nordlund, T. Mattila, Hillock formation on ion-irradiated graphite surfaces, Radiat. Eff. Defects Solids 142 (1–4) (1997) 459–469.
[21] N. Dilawar, R. Kapil, V. Vankar, D. Avasthi, D. Kabiraj, G. Mehta, Radiation hardness of polycrystalline diamond thin films irradiated with 100 MeV I 7+ ions, Thin Solid Films 305 (1) (1997) 88–94.
[22] W. Zhu, G. Kochanski, S. Jin, L. Seibles, D. Jacobson, M. McCormack, A. White, Electron field emission from ion-implanted diamond, Appl. Phys. Lett. 67 (8) (1995) 1157–1159.
[23] A. Dunlop, G. Jaskierowicz, P. Ossi, S. Della-Negra, Transformation of graphite into nanodiamond following extreme electronic excitations, Phys. Rev. B 76 (15) (2007) 155403.
[24] T. Makgato, E. Sideras-Haddad, S. Shrivastava, T. Schenkel, R. Ritter, G. Kowarik, F. Aumayr, J. Crespo López-Urrutia, S. Bernitt, C. Beilmann, et al., Highly charged ion impact induced nanodefects in diamond, Nucl. Instrum. Methods Phys. B 314 (2013) 135–139.
[25] S. Prawer, R. Kalish, Ion-beam-induced transformation of diamond, Phys. Rev. B 51 (22) (1995) 15711.
[26] J. Buchan, M. Robinson, H. Christie, D. Roach, D. Ross, N. Marks, Molecular dynamics simulation of radiation damage cascades in diamond, J. Appl. Phys. 117 (24) (2015) 245901.
[27] X.-M. Bai, A.F. Voter, R.G. Hoagland, M. Nastasi, B.P. Uberuaga, Efficient annealing of radiation damage near grain boundaries via interstitial emission, Science 327 (5973) (2010) 1631–1634.
[28] Y. Chimi, A. Iwase, N. Ishikawa, M. Kobiyama, T. Inami, S. Okuda, Accumulation

and recovery of defects in ion-irradiated nanocrystalline gold, J. Nucl. Mater. 297 (3) (2001) 355–357.
[29] H. Kurishita, S. Kobayashi, K. Nakai, T. Ogawa, A. Hasegawa, K. Abe, H. Arakawa, S. Matsuo, T. Takida, K. Takebe, et al., Development of ultra-fine grained W–(0.25–0.8) wt% TiC and its superior resistance to neutron and 3MeV He-ion irradiations, J. Nucl. Mater. 377 (1) (2008) 34–40.
[30] F. Valencia, J.D. Mella, R.I. González, M. Kiwi, E.M. Bringa, Confinement effects in irradiation of nanocrystalline diamond, Carbon 93 (2015) 458–464.
[31] S. Kidalov, F. Shakhov, A. Vul, Thermal conductivity of nanocomposites based on diamonds and nanodiamonds, Diam. Relat. Mater. 16 (12) (2007) 2063–2066 proc. Joint Int. Conf.: Nanocarbon and Nanodiamond 2006.
[32] S. Kidalov, F. Shakhov, A. Vul, Thermal conductivity of sintered nanodiamonds and microdiamonds, Diam. Relat. Mater. 17 (45) (2008) 844–847.
[33] H. Dong, B. Wen, R. Melnik, Relative importance of grain boundaries and size effects in thermal conductivity of nanocrystalline materials, Sci. Rep. 4 (2014) 7037.
[34] S.J. Stuart, A.B. Tutein, J.A. Harrison, A reactive potential for hydrocarbons with intermolecular interactions, J. Chem. Phys. 112 (14) (2000) 6472–6486.
[35] S. Plimpton, Fast parallel algorithms for short-range molecular dynamics, J. Comput. Phys. 117 (1) (1995) 1–19.
[36] E.M. Bringa, A. Caro, Y. Wang, M. Victoria, J.M. McNaney, B.A. Remington, R.F. Smith, B.R. Torralva, H. Van Swygenhoven, Ultrahigh strength in nanocrystalline materials under shock loading, Science 309 (5742) (2005) 1838–1841.
[37] E.M. Bringa, R.E. Johnson, M. Jakas, Molecular-dynamics simulations of electronic sputtering, Phys. Rev. B 60 (1999) 15107–15116.
[38] N.W. Lima, L.I. Gutierres, R.I. Gonzalez, S. Muller, R.S. Thomaz, E.M. Bringa, R.M. Papaléo, Molecular dynamics simulation of polymerlike thin films irradiated by fast ions: a comparison between FENE and Lennard-Jones potentials, Phys. Rev. B 94 (2016) 195417.
[39] G. Szenes, Uniform behavior of insulators irradiated by swift heavy ions, Nucl. Instrum. Methods Phys. B 354 (2015) 47–50.
[40] B. Afra, M. Rodriguez, C. Trautmann, O. Pakarinen, F. Djurabekova, K. Nordlund, T. Bierschenk, R. Giulian, M.C. Ridgway, G. Rizza, et al., SAXS investigations of the morphology of swift heavy ion tracks in α-quartz, J. Phys. Condens. Matter 25 (4) (2012) 045006.
[41] D.M. Follstaedt, A.K. Norman, P. Rossi, B.L. Doyle, F.D. McDaniel, E.M. Bringa, High-energy ion tracks in thin films, Nucl. Instrum. Methods Phys. B 242 (1) (2006) 79–81.
[42] L. Chun-E, X. Jian-Ming, W. Yu-Gang, Z. Yan-Wen, Molecular dynamics simulation of latent track formation in α-quartz, Chin. Phys. C 37 (3) (2013) 038201.
[43] R. Devanathan, P. Durham, J. Du, L.R. Corrales, E.M. Bringa, Molecular dynamics simulation of amorphization in forsterite by cosmic rays, Nucl. Instrum. Methods Phys. B 255 (1) (2007) 172–176.
[44] C. Scott, R. Smith, K. Sickafus, Surface topography induced by swift heavy ion impacts, Nucl. Instrum. Methods Phys. B 269 (14) (2011) 1625–1629.
[45] P. Sigmund, C. Claussen, Sputtering from elastic-collision spikes in heavy-ion-bombarded metals, J. Appl. Phys. 52 (2) (1981) 990–993.
[46] M.M. Jakas, E.M. Bringa, Thermal-spike theory of sputtering: the influence of elastic waves in a one-dimensional cylindrical spike, Phys. Rev. B 62 (2) (2000) 824.
[47] O.J. Tucker, D.S. Ivanov, L.V. Zhigilei, R.E. Johnson, E.M. Bringa, Molecular dynamics simulation of sputtering from a cylindrical track: EAM versus pair potentials, Nucl. Instrum. Methods Phys. B 228 (1) (2005) 163–169.